nature photonics

SUPPLEMENTARY INFORMATION

https://doi.org/10.1038/s41566-020-0589-x

In the format provided by the authors and unedited.

Demonstration of sub-3 ps temporal resolution with a superconducting nanowire single-photon detector

Boris Korzh[1,9] ✉, Qing-Yuan Zhao[2,9], Jason P. Allmaras[1,3], Simone Frasca[1], Travis M. Autry[4], Eric A. Bersin[1,2], Andrew D. Beyer[1], Ryan M. Briggs[1], Bruce Bumble[1], Marco Colangelo[2], Garrison M. Crouch[1], Andrew E. Dane[2], Thomas Gerrits[4], Adriana E. Lita[4], Francesco Marsili[1], Galan Moody[4], Cristián Peña[5,6], Edward Ramirez[1,7], Jake D. Rezac[4], Neil Sinclair[6], Martin J. Stevens[4], Angel E. Velasco[1], Varun B. Verma[4], Emma E. Wollman[1], Si Xie[6], Di Zhu[2], Paul D. Hale[4], Maria Spiropulu[6], Kevin L. Silverman[4], Richard P. Mirin[4], Sae Woo Nam[4], Alexander G. Kozorezov[8], Matthew D. Shaw[1] and Karl K. Berggren[2]

[1]Jet Propulsion Laboratory, California Institute of Technology, Pasadena, CA, USA. [2]Department of Electrical Engineering and Computer Science, Massachusetts Institute of Technology, Cambridge, MA, USA. [3]Department of Applied Physics, California Institute of Technology, Pasadena, CA, USA. [4]National Institute of Standards and Technology, Boulder, CO, USA. [5]Fermi National Accelerator Laboratory, Batavia, IL, USA. [6]Division of Physics, Mathematics and Astronomy, California Institute of Technology, Pasadena, CA, USA. [7]Department of Electrical and Computer Engineering, California State University, Los Angeles, CA, USA. [8]Department of Physics, Lancaster University, Lancaster, UK. [9]These authors contributed equally: Boris Korzh, Qing-Yuan Zhao. ✉e-mail: bkorzh@jpl.caltech.edu

Demonstration of sub-3 ps temporal resolution with a superconducting nanowire single-photon detector

Boris Korzh[1]*, Qing-Yuan Zhao[2], Jason P. Allmaras[1,3], Simone Frasca[1], Travis M. Autry[4], Eric A. Bersin[1,2], Andrew D. Beyer[1], Ryan M. Briggs[1], Bruce Bumble[1], Marco Colangelo[2], Garrison M. Crouch[1], Andrew E. Dane[2], Thomas Gerrits[4], Adriana E. Lita[4], Francesco Marsili[1], Galan Moody[4], Cristián Pena[5,6], Edward Ramirez[1], Jake D. Rezac[4], Neil Sinclair[5], Martin J. Stevens[4], Angel E. Velasco[1], Varun B. Verma[4], Emma E. Wollman[1], Si Xie[5], Di Zhu[2], Paul D. Hale[4], Maria Spiropulu[5], Kevin L. Silverman[4], Richard P. Mirin[4], Sae Woo Nam[4], Alexander G. Kozorezov[7], Matthew D. Shaw[1] and Karl K. Berggren[2]

[1]*Jet Propulsion Laboratory, California Institute of Technology, Pasadena, California 91109, USA*

[2]*Department of Electrical Engineering and Computer Science, Massachusetts Institute of Technology, Cambridge, Massachusetts 02139, USA*

[3]*Department of Applied Physics, California Institute of Technology, Pasadena, California 91125, USA*

[4]*National Institute of Standards and Technology, Boulder, Colorado 80305, USA*

[5]*Division of Physics, Mathematics and Astronomy, California Institute of Technology, Pasadena, California 91125, USA*

[6]*Fermi National Accelerator Laboratory, Batavia, Illinois 60510, USA*

[7]*Department of Physics, Lancaster University, Lancaster, LA1 4YB, UK*

*Correspondence to: bkorzh@jpl.caltech.edu

Supplementary Note 1 | Latency to slew rate correlation. In order to avoid current crowding,[1] the nanowire is connected to the wire terminals with a short tapering section (see Figure 2 in the main manuscript). If a photon detection occurs in this region of widening nanowire, then the overall detection latency will increase (see Figure 3 in main text for effect of nanowire width at a fixed bias current), resulting in a larger number of tail of events in the IRF histogram. As evidence towards this hypothesis we have studied the correlation between the shot-to-shot slew rate of the SNSPD signals and the threshold crossing delay. An additional effect of a detection in a widening section of a nanowire is that during the hotspot expansion, the final resistance will be lower and since the slew rate is proportional to the kinetic inductance (fixed) divided by the hotspot resistance. It means that the slew rate will be lower for detection in the tapering sections. It is therefore possible to use the slew rate as an indicator of whether the detection happened in the tapering sections. Supplementary Figure 1a confirms this since there is a correlation between the slew rate and detection delay – the lower the slew rate, the wider the nanowire section responsible for the detection and hence the larger the delay. In order to infer how the jitter histogram would look like without the effect of the tapering sections we set a threshold in the slew rate such as to reduce the contribution of the tail events. Supplementary Figure 1b shows the resulting IRF with and without the slew rate thresholding, achieving a significant reduction of the tail events. Note that the tail still deviated from exponential, which is expected based on the simulations (see Supplementary Note 3). This analysis indicates that for best performance the light absorption should be concentrated away from tapering sections and bends.

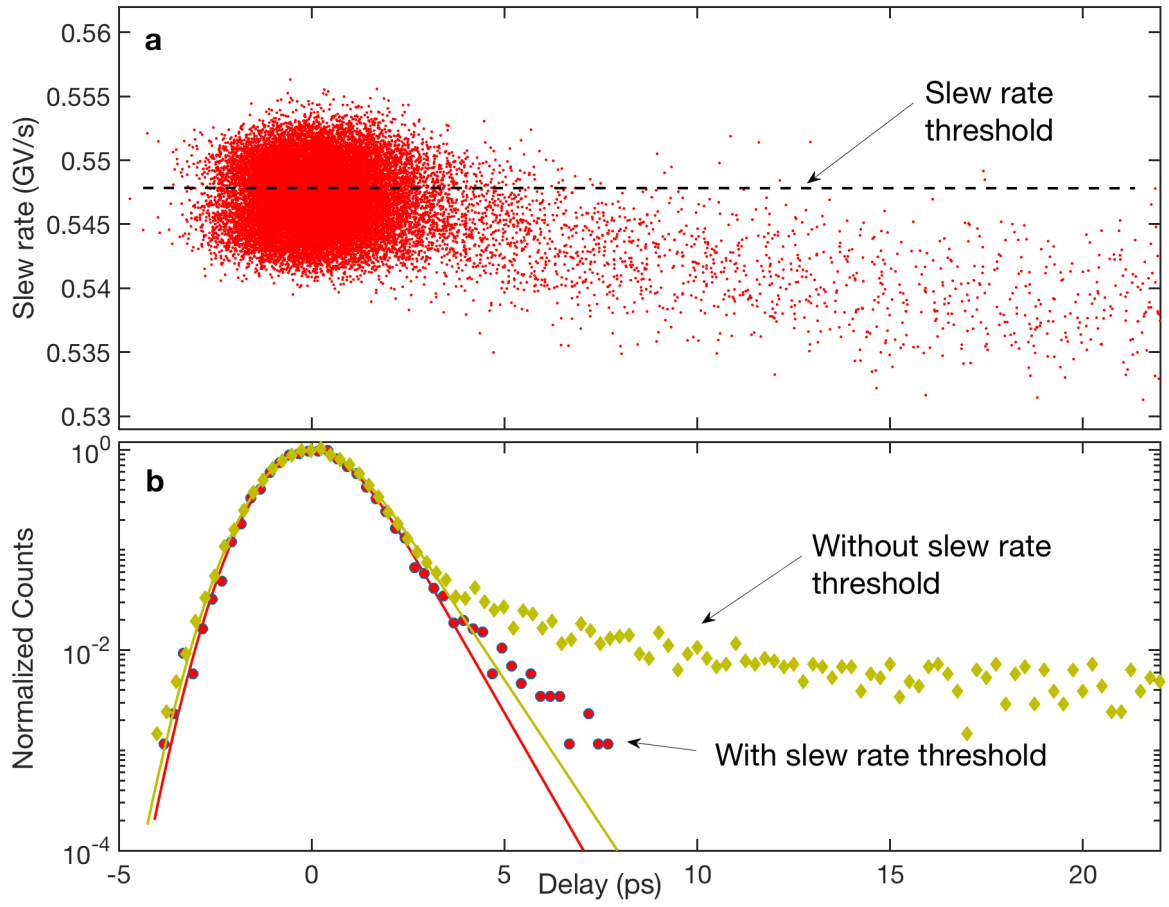

Supplementary Figure 1. a, Correlation between the slew rate of the detection signal and the threshold crossing delay for the 120 nm-wide nanowire biased at the maximum bias current and illuminated with 532 nm light. When excluding all detection below the slew rate threshold indicated in (a) the tail events considerably reduce **b,** indicating that the tapering sections of the nanowire are the main contributing factors to the histogram tail. The exponentially modified Gaussian fit deviates from the experimental data even with the slew rate thresholding, however, it provides an adequate fit for extraction of the FWHM of the distribution.

Supplementary Note 2 | Changes in the IRF tail for short wavelengths. When characterizing the 120 nm-wide nanowire, we noticed that the tail of the distribution for the shortest wavelength light has a significantly different shape, especially at low bias currents. Supplementary Figure 2 shows a comparison of the instrument response functions for three wavelengths (273 nm, 400 nm and 800 nm) for different bias currents. At the lowest bias current of 13 μA, there is a systematic deviation (below 0.25 of the peak) for the 273 nm wavelength data (Supplementary Figure 2a). This deviation decreases at longer wavelengths (Supplementary Figure 2b, c). The origin of this effect can be attributed to differing detection latency for various transverse coordinates of absorption in the nanowire.[2] This effect is known as 'transverse geometric' jitter.

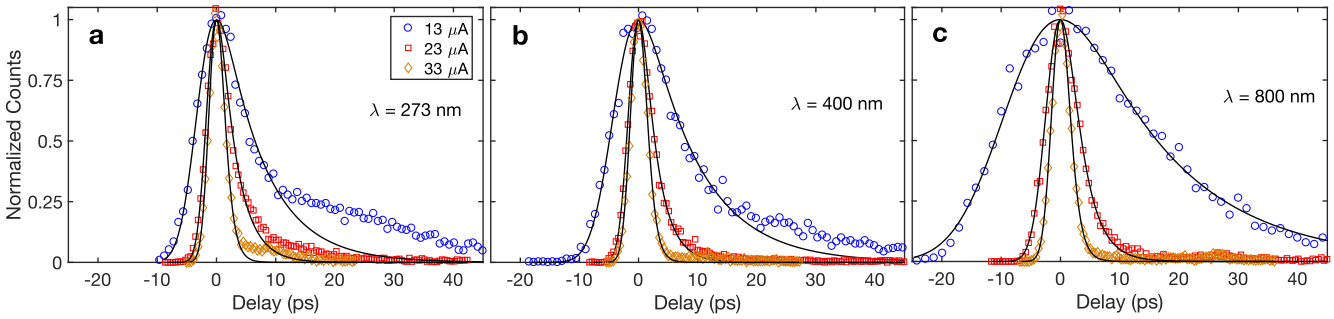

Supplementary Figure 2. Instrument response functions for the 120 nm nanowire biased at 13 μA (circles), 23 μA (squares) and 33 μA (diamonds). Data for the 273 nm (a), 400 nm (b) and 800 nm (c) is shown for comparison.

Supplementary Note 3 | Fitting the experimental data with simulations. The general features a)-d) of the detector latency function discussed in Methods: Detection latency simulations are sufficient for qualitative analysis of the experimental data, but numerical simulation is required to determine the functional form of the latency. To simulate latency curves we numerically solved the system of generalized TDGL equations together with energy balance equations and current continuity equations subject to the appropriate boundary conditions[3]. We used the hotbelt detection model[4–8] and 1D-geometry for simplicity and clarity of presentation, but verified that the results are consistent with the results of the full 2D hotspot detection scenario.[2,7,9,10] The use of the generalized TDGL equations[11] with less stringent validity conditions than the standard TDGL is more appropriate for simulating the suppression of the gap over extended intervals of time when both the superconducting order parameter and the energy gap remain finite. The major parameters of the NbN SNSPD used for this simulation are shown in the Supplementary Table 1. The simulated latency results for the 80 nm SNSPD are shown in Supplementary Figure 3.

It is seen that all the calculated latency curves have features a) to d) described in the Methods of the main manuscript. The bell-shaped curve above horizontal axis in Supplementary Figure 4 schematically shows the normal distribution density of energy deposition into electron system following photon absorption and the right-skewed bell-shaped curve on the right schematically shows the origin and shape of timing jitter distribution originating from fluctuations of detector latency.

i. Shape of jitter distributions. It is easy to see from this figure that because of c) the shape of jitter distribution is distorted Gaussian with long tail at higher delays consistent with data, see Figure 1 of the main manuscript.

ii. Bias current dependence of the jitter and detection latency difference. For any fixed photon energy both latency and jitter FWHM increase with decreasing current, as in Figures 3a and c of the main manuscript.

iii. Wavelength dependence of the jitter. For any bias current because of a)-c) both latency and jitter FWHM decrease when photon energy increases as in Figure 4a of the main manuscript.

iv. Width of nanowire dependence. The data in Figure 3 of the main manuscript are easily understood as a result of scaling of current and deposition energy densities with the nanowire width.

The model used to simulate the detection latency difference shown in Figure 3c of the main manuscript simultaneously predicts the PCR and IRF for different bias conditions and photon energies. With the three fitting parameters $\chi = 0.667$, $\sigma_{1550} = 100$ meV, and $\tau_{ee}(T_c) = 6$ ps, we fit these three key experimental metrics for both the 80 nm and 60 nm wide samples. We note that with these fitting parameters, the high energy tail of the absorbed energy distribution can extend beyond the full photon energy for low photon energies, which is an unphysical result of using the simplified 1D model. If a small contribution of the fluctuations comes from non-uniformities ($\sigma_{1550,\mathrm{n-u}}$) as treated in Ref.[3] such that $\sigma_{1550,\mathrm{Fano}} = 92$ meV and $\sigma_{1550,\mathrm{n-u}} = 40$ meV, this effect is eliminated without changing the quality of the fit. The PCR results are shown for 1550 nm and 775 nm photons in Supplementary Figure 3. The comparison of the IRF for the 80 nm wire is shown in Supplementary Figure 4.

Description	**Symbol**	**Value**
Nanowire width	W	80 nm
Nanowire thickness	d	7 nm
Critical temperature	T_c	8.65 K
Diffusion coefficient	D	0.5 $\mathrm{cm}^2 s^{-1}$
Sheet resistance	R_{sq}	608 Ω/□
Phonon parameter	γ	60
Hotbelt length	L	40 nm
Inelastic electron-electron scattering time at T_c	$\tau_{ee}(T_c)$	6 ps
Electron-phonon coupling time at T_c	$\tau_{ep}(T_c)$	24.7 ps
Phonon escape time	τ_{esc}	20 ps
Mean fraction of the photon energy deposited in the nanowire	χ	0.667
Standard deviation due to Fano fluctuations	$\sigma_{1550,Fano}$	92 meV
Standard deviation due to spatial non-uniformity[3]	$\sigma_{1550,n-u}$	40 meV

Supplementary Table 1. Parameters for simulation of latency in the 80 nm SNSPD.

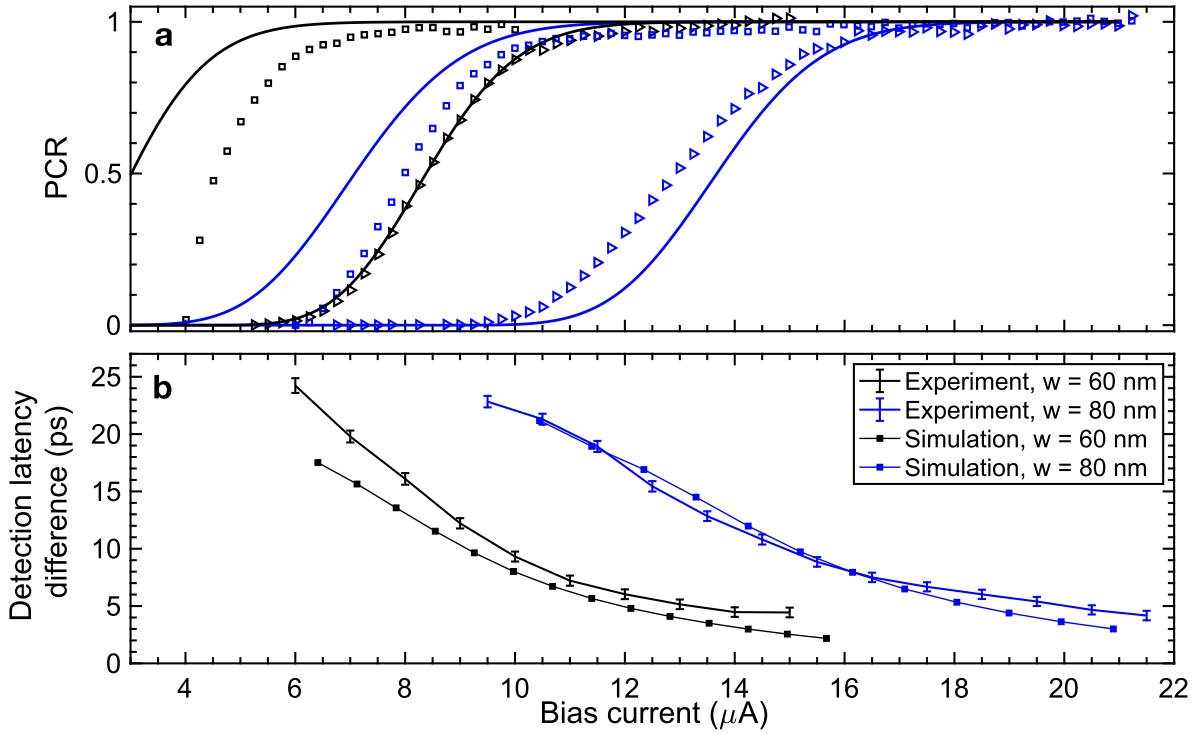

Supplementary Figure 3 | **a,** Normalized *PCR* for 80 nm (blue symbols) and 60 nm (black symbols) samples for 775 nm light (squares) and 1550 nm light (triangles) compared to simulation (solid lines). **b,** Detection delay difference for 80 nm (blue) and 60 nm (black) samples compared to simulation (squares

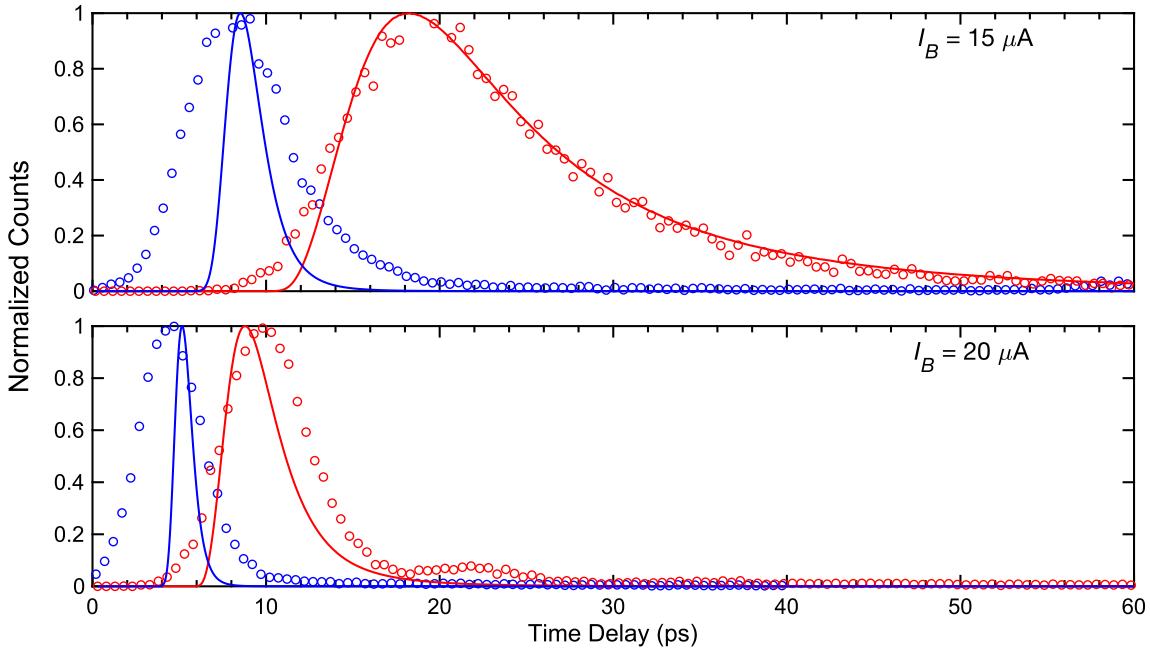

Supplementary Figure 4 | Comparison of simulated IRF with experiment for the 80 nm wide nanowire at bias for **a,** 15 μA bias current and **b,** 20 μA bias current. Solid lines indicate the simulated IRF while the symbols correspond to the experimental data. The data in red corresponds to a 1550 nm photon, while blue data corresponds to a 775 nm photon. This illustrates the changes in the relative latency between the two photon energies as well as the change in the IRF width. The agreement with experimental data is not perfect indicating a need for further development of the numerical model.

References

1. Clem, J. R. & Berggren, K. K. Geometry-dependent critical currents in superconducting nanocircuits. *Phys. Rev. B* **84**, 174510 (2011).
2. Vodolazov, D. Y. Minimal Timing Jitter in Superconducting Nanowire Single-Photon Detectors. *Phys. Rev. Appl.* **11**, 014016 (2019).
3. Allmaras, J. P., Kozorezov, A. G., Korzh, B. A., Berggren, K. K. & Shaw, M. D. Intrinsic Timing Jitter and Latency in Superconducting Nanowire Single-photon Detectors. *Phys. Rev. Appl.* **11**, 034062 (2019).
4. Marsili, F. *et al.* Hotspot relaxation dynamics in a current-carrying superconductor. *Phys. Rev. B* **93**, 094518 (2016).
5. Bulaevskii, L. N., Graf, M. J., Batista, C. D. & Kogan, V. G. Vortex-induced dissipation in narrow current-biased thin-film superconducting strips. *Phys. Rev. B* **83**, 144526 (2011).
6. Kozorezov, A. G. *et al.* Quasiparticle recombination in hotspots in superconducting current-carrying nanowires. *Phys. Rev. B* **92**, 064504 (2015).
7. Vodolazov, D. Y. Single-Photon Detection by a Dirty Current-Carrying Superconducting Strip Based on the Kinetic-Equation Approach. *Phys. Rev. Appl.* **7**, 034014 (2017).
8. Kozorezov, A. G. *et al.* Fano fluctuations in superconducting-nanowire single-photon detectors. *Phys. Rev. B* **96**, 054507 (2017).
9. Zotova, A. N. & Vodolazov, D. Y. Photon detection by current-carrying superconducting film: A time-dependent Ginzburg-Landau approach. *Phys. Rev. B* **85**, 024509 (2012).
10. Engel, A., Lonsky, J., Zhang, X. & Schilling, A. Detection Mechanism in SNSPD: Numerical Results of a Conceptually Simple, Yet Powerful Detection Model. *IEEE Trans. Appl. Supercond.* **25**, 2200407 (2015).
11. Kopnin, N. B. *Theory of Nonequilibrium Superconductivity*. (Oxford University Press, 2001).

12. Frasca, S. *et al.* Determining the depairing current in superconducting nanowire single-photon detectors. *Phys. Rev. B* **100**, 054520 (2019).